Monthly Notices of the ROYAL ASTRONOMICAL SOCIETY

MNRAS **536,** 3421–3430 (2025) https://doi.org/10.1093/mnras/stae2755
Advance Access publication 2024 December 13

Long-term optical variations in Swift J1858.6–0814: evidence for ablation and comparisons to radio properties

L. Rhodes [1]★ D. M. Russell,[2] P. Saikia,[2] K. Alabarta [2], J. van den Eijnden [3], A. H. Knight [4], M. C. Baglio[5] and F. Lewis[6,7]

[1]*Astrophysics, Department of Physics, University of Oxford, Denys Wilkinson Building, Keble Road, Oxford OX1 3RH, UK*
[2]*Center for Astrophysics and Space Science (CASS), New York University Abu Dhabi, PO Box 129188 Abu Dhabi, UAE*
[3]*Department of Physics, University of Warwick, Coventry CV4 7AL, UK*
[4]*Centre for Extragalactic Astronomy, Department of Physics, Durham University, South Road, Durham DH1 3LE, UK*
[5]*INAF – Osservatorio Astronomico di Brera, Via Bianchi 46, I-23807 Merate (LC), Italy*
[6]*Faulkes Telescope Project, School of Physics and Astronomy, Cardiff University, The Parade, Cardiff, CF24 3AA Wales, UK*
[7]*The Schools' Observatory, Astrophysics Research Institute, Liverpool John Moores University, 146 Brownlow Hill, Liverpool L3 5RF, UK*

Accepted 2024 December 12. Received 2024 December 10; in original form 2024 August 23

ABSTRACT

We present optical monitoring of the neutron star low-mass X-ray binary Swift J1858.6–0814 during its 2018–2020 outburst and subsequent quiescence. We find that there was strong optical variability present throughout the entire outburst period covered by our monitoring, while the average flux remained steady. The optical spectral energy distribution is blue on most dates, consistent with emission from an accretion disc, interspersed by occasional red flares, likely due to optically thin synchrotron emission. We find that the fractional rms variability has comparable amplitudes in the radio and optical bands. This implies that the long-term variability is likely to be due to accretion changes, seen at optical wavelengths, that propagate into the jet, seen at radio frequencies. We find that the optical flux varies asymmetrically about the orbital period, peaking at phase ∼0.7, with a modulation amplitude that is the same across all optical wavebands, suggesting that reprocessing off of the disc, companion star and ablated material is driving the phase dependence. The evidence of ablation found in X-ray binaries is vital in understanding the long-term evolution of neutron star X-ray binaries and how they evolve into (potentially isolated) millisecond pulsars.

Key words: accretion, accretion discs – ISM: jets and outflows – X-rays: binaries – X-rays: individual: Swift J1858.6–0814.

1 INTRODUCTION

Low-mass X-ray binaries (LMXBs) are binary systems made up of a compact object, either a black hole (BH) or neutron star (NS), and a low-mass stellar companion. Mass is transferred from the star to the compact object via Roche Lobe overflow through the inner Lagrange point. A given LMXB can go through a period of increased mass accretion rate called an 'outburst', producing luminous, variable emission from radio to X-ray energies, which can last between weeks and months (see e.g. Bahramian & Degenaar 2023, for a review). The earliest sign of an LMXB going into outburst is thought to be a sharp increase in optical flux (see Russell et al. 2019, and references therein). For BH LMXBs, near the beginning of the outburst, there is also a radio brightening accompanying an X-ray rise. During the hard state, named after the hard, power-law X-ray spectrum, any radio emission is thought to originate from a compact jet (Fender 2001). As the outburst evolves and the system transitions to a more X-ray-luminous, disc-dominated 'soft state', the radio emission is quenched (Fender, Belloni & Gallo 2004). However, for XRBs hosting NSs, this process is more complex. For example, the radio emission is not fully quenched when NS XRBs transition into soft state (see Migliari et al. 2004; Gusinskaia et al. 2017, for examples of radio detections and deep limits in the soft state, respectively). The origin of the optical emission in LMXBs is more complex because the total flux may be a combination of multiple components. During quiescence, the optical counterpart can be dominated by the companion star in the system, or by low level accretion activity (e.g. Greene, Bailyn & Orosz 2001; Zurita, Casares & Shahbaz 2003; Cantrell et al. 2010; Baglio et al. 2017, 2022). An associated jet contribution is seen rarely (Baglio et al. 2013; Plotkin et al. 2016; Russell et al. 2018). During outbursts, the observed emission is thought to be mostly a superposition of optical emission from the disc, reprocessed X-ray emission on the disc surface, and a jet component. Multifrequency optical data is required to interpret whether the emission is from the disc or jet as the two components are blue and red in colour, respectively (e.g. Corbel & Fender 2002; Greenhill, Giles & Coutures 2006; Russell, Fender & Jonker 2007; Rahoui et al. 2012). In addition to the long-term flux changes, many LMXBs also show shorter-term (sub-seconds to days) variability, corresponding to rapid changes in accretion rate, quasi-periodic oscillations from the inner accretion flow, flickering from the jet or bursting from the neutron star surface and inner accretion flow (e.g. Casella et al. 2010; Veledina, Poutanen & Vurm 2011; Bagnoli

★ E-mail: lauren.rhodes@mcgill.ca

et al. 2015; Gandhi et al. 2017; Malzac et al. 2018; Ingram & Motta 2019; Tetarenko et al. 2019).

NS LMXBs are thought to be progenitors to millisecond pulsars (MSPs), as confirmed by the discovery of the transitional MSP PSR J1023 + 0038 (Alpar et al. 1982; Wijnands & van der Klis 1998; Archibald et al. 2009; Papitto et al. 2013). Some MSPs in binary systems are known as 'spider pulsars' thanks to evidence of ablation of the stellar companion by the pulsar wind. It may be possible for complete ablation of the stellar companion to occur resulting in an isolated MSP (Roberts 2012). More recently, evidence of ablation has been found in NS LMXBs whilst in outburst where ablation is thought to be driven by X-ray irradiation rather than the pulsar wind, thus suggesting that ablation is a more common process in NS binary systems than was originally thought, including a recently discovered system *Swift* J1858.6–0814 (Knight et al. 2023).

1.1 *Swift* J1858.6–0814

Swift J1858.6–0814 (hereafter J1858) was first reported by the Neil Gehrels *Swift* Observatory – Burst Alert Telescope (BAT) as a Galactic X-ray transient on 25 October 2018 (MJD 58416, Krimm et al. 2018, the dotted vertical line in Fig. 1). The UV, optical and radio counterparts were soon identified (Bright et al. 2018; Kennea & Krimm 2018; Vasilopoulos, Bailyn & Milburn 2018). The source remained in a highly variable, flaring state until February 2020, the system underwent a state transition (the vertical dashed line in fig. 1 Buisson et al. 2020b) finally by May 2020 (MJD 58970) J1858 was in a quiescent state (Parikh, Wijnands & Altamirano 2020; Saikia et al. 2020).

Given its highly variable nature, J1858 has been the subject of many in-depth campaigns at X-ray energies. We highlight two findings of interest for their relevance for the work presented here: (1) type-I X-ray bursts and (2) X-ray eclipses. The former confirmed the nature of the compact object as a neutron star and the latter provided strong constraints on the system inclination of $\sim 81^{\circ}$ (Buisson et al. 2020a, 2021; Knight, Ingram & Middleton 2022; Knight et al. 2023; Vincentelli et al. 2023). Knight et al. (2022) also found evidence of ablation of the companion star, i.e. the removal of material from the surface of the companion star mostly likely by high energy radiation from the inner accretion flow, analogous to the pulsar wind-driven ablation found in spider pulsars (Stappers et al. 2001).

There have been a number of targeted short time-scale variability studies of J1858 across all wavelength bands (e.g. den Eijnden et al. 2020; Castro Segura et al. 2022; Shahbaz et al. 2023). The long-term radio behaviour of J1858 is best described by an initial flare, followed by a variable, persistent source that remained until the system underwent a state transition. The radio source was attributed to a compact jet, determined by a flat/positive ($\alpha > 0$, flux density $\propto \nu^{\alpha}$) spectral index (den Eijnden et al. 2020; Rhodes et al. 2022). On shorter time-scales of $\sim$ minutes, the radio emission was highly variable with root mean square (rms) variability measurements ranging between 15 and 60 per cent across the outburst. The rapid variability was accompanied by a broader range of spectral index measurements swapping between optically thick and optically thin synchrotron spectra (Rhodes et al. 2022; Vincentelli et al. 2023). The optically thick-thin transitions were interpreted as successive jet ejections as opposed to the expected canonical hard state jet.

At optical wavelengths, the emission is dominated by the accretion disc. Perhaps the most interesting characteristic of the optical data published thus far is the rapid variability as reported by Shahbaz et al. (2023). Similar behaviour was also reported by Baglio et al. (2018), Paice et al. (2018), Rajwade et al. (2018), and Vincentelli et al. (2023). The flaring behaviour is split into 'blue' and 'red' flares. The red flares are interpreted as originating from the jet, they are shorter in duration (10s of seconds) and smaller in amplitude. However, as of yet no direct comparisons have been made with the radio properties of the system. The brighter, longer blue flares (100–400 s) are consistent with an accretion disc spectrum (Muñoz-Darias et al. 2020; Castro Segura et al. 2022).

In this paper, we present new long-term optical monitoring of J1858 from the Las Cumbres Observatory and discuss the variability properties of the source compared to what has been observed at radio frequencies. Section 2 lays out the optical observing campaign and recaps the radio monitoring programs for J1858. In Section 3, we present the results of our analysis of the optical data in both time and frequency space, comparing the optical and radio variability and spectral properties, before interpreting them within the picture of NS LMXBs and spider pulsars. Finally, in Section 5 we lay out our conclusions.

2 OBSERVATIONS

2.1 Faulkes telescope/LCO monitoring

We began monitoring *Swift* J1858.6–0814 with the 1-m and 2-m Las Cumbres Observatory (LCO; Brown et al. 2013) network of optical telescopes in November 2018, starting with some fast-timing observations with the 2-m Faulkes Telescope North (at Haleakala Observatory, Maui, Hawai'i, USA) on 2018 November 6 (initial results were presented in Baglio et al. 2018). Monitoring continued throughout the outburst using both 2-m Faulkes Telescopes (Faulkes Telescope South is located at Siding Spring Observatory, Australia) and the 1-m network, which includes nodes at Siding Spring Observatory (Australia), Cerro Tololo Inter-American Observatory (Chile), McDonald Observatory (Texas, USA), Teide Observatory (Tenerife, Canary Islands, Spain), and the South African Astronomical Observatory (SAAO, South Africa). The LCO network comprise of robotic telescopes optimized for research and education (e.g. Lewis 2018).

Imaging was carried out roughly weekly in the SDSS g', r', i' and PanSTARRS Y-band filters during the outburst, and continued in the i' band in quiescence after the outburst, as part of an on-going monitoring campaign of $\sim$50 LMXBs (Lewis et al. 2008) coordinated by the Faulkes Telescope Project. Exposure times were between 60 and 200 s. In addition, a sequence of 50 r'-band exposures were taken on 2018-11-06, with exposure times of 30 s (the time resolution was 46 s; Baglio et al. 2018). Data reduction and aperture photometry were carried out by the 'X-ray Binary New Early Warning System (XB-NEWS)' data analysis pipeline (Russell et al. 2019; Goodwin et al. 2020a). The pipeline downloads images and calibration data from the LCO archive, performs several quality control steps to reject any bad quality images, and computes an astrometric solution on each image using *Gaia* DR2[1] positions, and then performs aperture photometry of all the stars. The method described in Bramich & Freudling (2012) is used to solve for zero-point magnitude offsets between epochs, and multi-aperture photometry is used on the target. Flux calibration of all stars is achieved using the ATLAS All-Sky Stellar Reference Catalog (ATLAS-REFCAT2; Tonry et al. 2018)[2], which includes APASS, PanSTARRS DR1, and other catalogues to extract the magnitudes of the source. When the source is not detected above the detection threshold by the pipeline, XB-NEWS

[1] https://www.cosmos.esa.int/web/gaia/dr2
[2] https://archive.stsci.edu/prepds/atlas-refcat2/

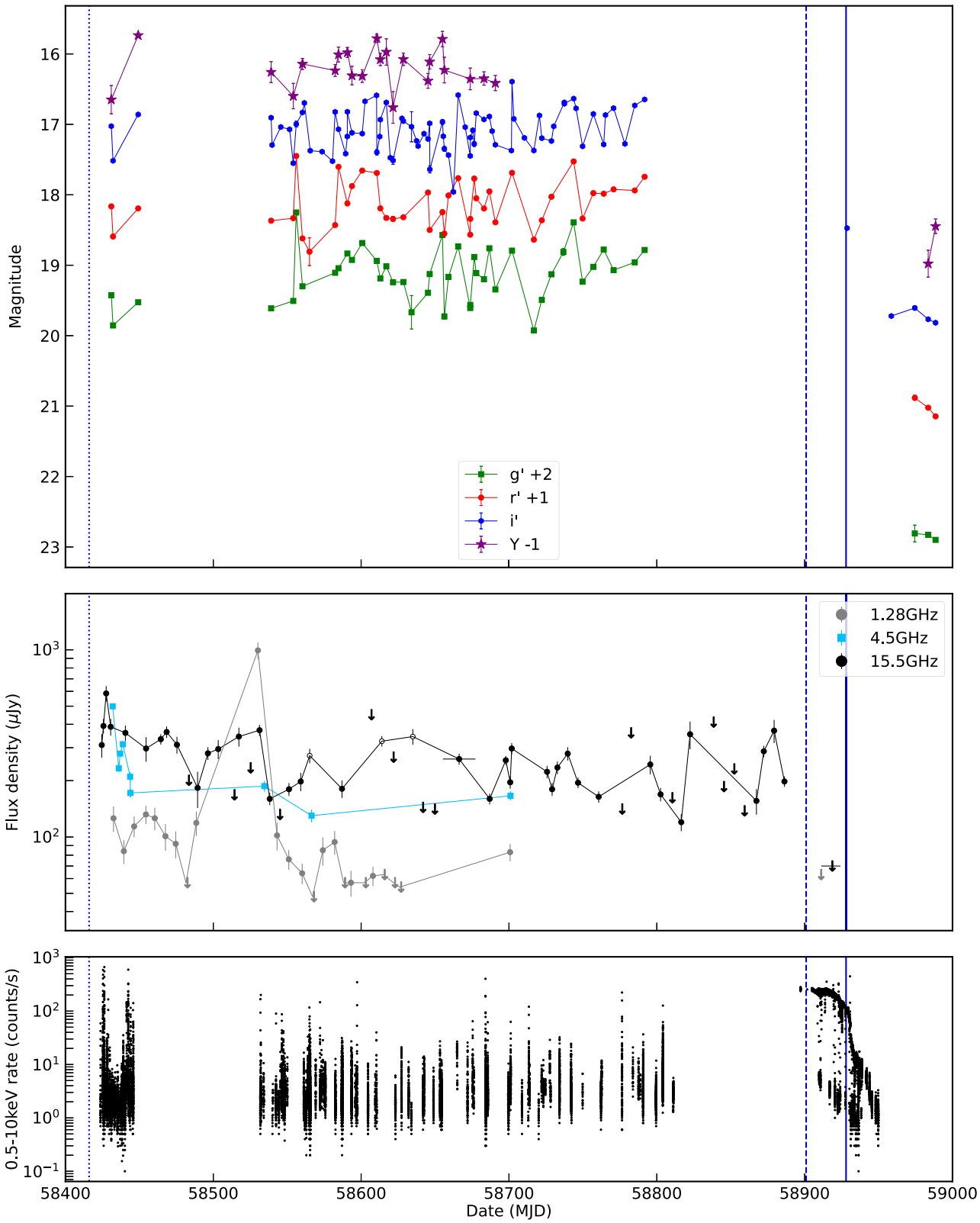

Figure 1. *Upper panel:* Optical light curves of the J1858 system during outburst and quiescence. Artificial offsets have been placed to make the data easier to visualize. The vertical dotted, dashed, and solid blue lines indicate the outburst's beginning, state transition, and return to quiescence, respectively. *Middle panel*: The radio data from van den Eijnden et al. (2020) and Rhodes et al. (2022). *Lower panel*: The 0.5–10 keV NICER light curve from Castro Segura et al. (2022).

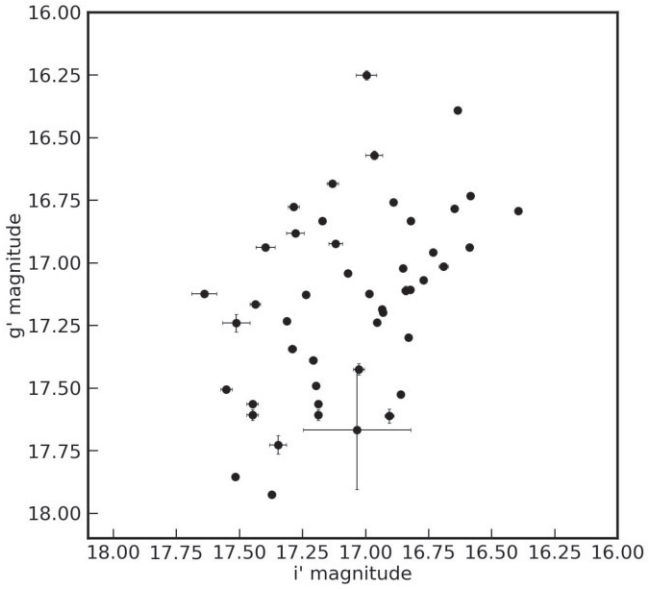

Figure 2. g' versus i' magnitude for observations made within the same night (most are taken within a few minutes during a filter sequence). There is evidence of a correlation but with considerable scatter, indicating that the variability time-scale is shorter than the time between observations in different filters.

performs forced photometry at the known location of the source. Magnitudes with errors > 0.25 mag are excluded as these are either very marginal detections or non-detections. Since XB-NEWS uses multi-epoch detections to derive a best-fitting position for the source, we report here the coordinates derived of *Swift* J1858.6–0814 by XB-NEWS, of RA = 18 58 34.905, Dec. = −08 14 14.94 (J2000; with an error of less than ~ 0.2 arcsec from catalogue cross-calibration uncertainties). This is consistent (within 1 arcsec) with the *Swift* UVOT position (Kennea & Krimm 2018) and the PanSTARRS position (within 0.2 arcsec; object ID 98112846453925483; observed during quiescence).

2.2 Radio data

We use radio observations presented in den Eijnden et al. (2020) and Rhodes et al. (2022), to contextualize the optical data described in Section 2.1. The data from these two publications cover both long-term monitoring campaigns and short-term variability studies. The data we use from these studies covers three frequencies: 1.28 GHz (MeerKAT), 4.5 GHz (the VLA) and 15.5 GHz (AMI-LA). Variability was observed on both long (week–month) and short (minute) time-scales. Across the observing campaigns, the radio spectrum was consistent with optically thick emission i.e. a steep spectrum ($\alpha > 0$).

3 RESULTS

3.1 Light curves

Fig. 1 shows a summary of J1858's outburst through its multiwavelength light curves. Across all wavebands there is significant and rapid variability. The upper panel of Fig. 1 shows the optical data of J1858 from our observing campaign starting from MJD 58 431 (9th November 2018) and continuing until MJD 60 126 (9th May 2020). The central panel in Fig. 1 shows the long-term radio monitoring

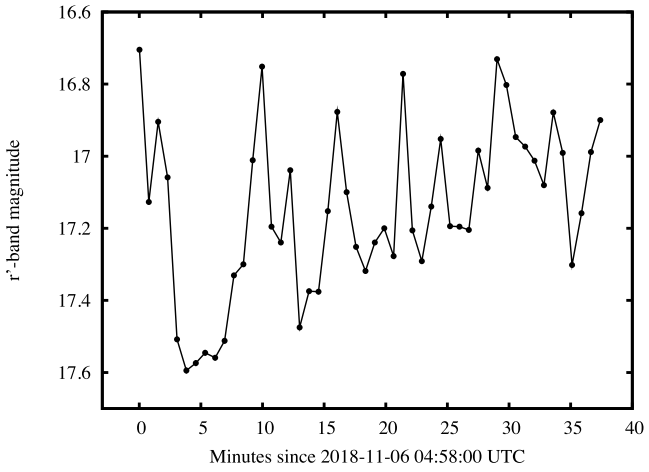

Figure 3. Short-term optical variability observed near the start of the outburst, demonstrating that the source can vary as much as 0.9 mag on time-scales of a few minutes. Magnitude errors are plotted, but are generally smaller than the symbols. Flares and dips on these time-scales are similar to those reported in Muñoz-Darias et al. (2020), Vincentelli et al. (2023), and Shahbaz et al. (2023).

from den Eijnden et al. (2020) and Rhodes et al. (2022). The lower panel shows the 0.5–10 keV NICER X-ray light curve from Castro Segura et al. (2022). In the X-ray light curve, the transition from the flaring to steady state (denoted by the vertical dashed line) and the fade into quiescence (the solid vertical line) are both very clear.

X-ray binary optical light curves typically follow a the typical fast rise, exponential decay trend (e.g. Muñoz-Darias et al. 2013; Goodwin et al. 2020b; Carotenuto et al. 2021; Saikia et al. 2023a). In the case of J1858, there are no clear long-term trends, the optical counterpart in the upper panel of Fig. 1, has a mean magnitude in g', r', i', and y bands of 17.1±0.4, 17.1±0.3, 17.1±0.3, and 17.2±0.3, respectively, (not corrected for interstellar extinction); the uncertainties are 1σ and for comparison, the average uncertainty on a single data point is 0.04 mag. The uncertainty on the average magnitude reflects the significant variability in each band. We find that the amplitude of variability is strongly correlated with frequency, such that the highest frequency has the highest amplitude and the lowest frequency has the lowest amplitude. The fractional rms ($F_{\rm rms}$) variability (Vaughan et al. 2003) across our 400 d-long observing campaign of ∼weekly observations is 19 ± 3 per cent in y-band and 35.5 ± 0.6 per cent in g' band.

Between MJD 58 700 and 58750, there are potential signs of correlated behaviour across the g', r', and i' bands. However, across the outburst, we find only weakly correlated behaviour between all or any two given bands (as demonstrated by the large scatter in Fig. 2). This suggests that the intrinsic variability time-scale is shorter than the time taken to observe in two successive bands. This is further demonstrated in Figs 2 and 3. In Fig. 2, for a given g' or i'-band measurement, there is about one magnitude of scatter in the other band. Fig. 3 shows the results of a fast photometry observation (36-s time resolution; Table 1) with the 2-m Faulkes Telescope North (see also Baglio et al. 2018). We observe flaring behaviour on minute time-scales where the observed flux varied by as much as 0.9 mag, which is consistent with the findings in Fig. 2.

Around MJD 58928, J1858 fades towards quiescence (Saikia et al. 2020), during which time, we only have observations in r', i', and y bands. In quiescence, the source is between 2.5 and 3 mag fainter than during outburst, considering only the epochs with the best seeing

Table 1. $F_{\rm rms}$ variability values over the broadband spectrum of J1858, on various time-scales, during the outburst. For the radio values we consider only the detections, and remove the milli-Jansky flare from the MeerKAT data set. For a sequence of observations, the frequency range probed (column 8) is the frequency corresponding to the total length of time of the sequence (minimum) and the time resolution (maximum).

Regime	Waveband	Central ν (Hz)	Facility	MJD range	$F_{\rm rms}$ (per cent)	Cadence	Frequency range (Hz)	Reference
Radio	*L* band	1.28×10^9	MeerKAT	58432–58700	20±4	7 d	$2.4 \times 10^{-8} - 1.9 \times 10^{-6}$	Rhodes et al. (2022)
Radio	*C* band	4.5×10^9	VLA	58431–58701	46±10	1 d	$4.3 \times 10^{-8} - 6.7 \times 10^{-5}$	den Eijnden et al. (2020)
Radio	*Ku* band	1.55×10^{10}	AMI-LA	58424–58886	33±2	∼7d	$2.5 \times 10^{-8} - 1.1 \times 10^{-5}$	Rhodes et al. (2022)
Optical	g'-band	6.29×10^{14}	LCO	58431–58791	35.5 ± 0.6	∼7d	$3.2 \times 10^{-8} - 2.9 \times 10^{-4}$	This work
Optical	r'-band	4.83×10^{14}	LCO	58431–58791	31.4 ± 0.4	∼11d	$2.7 \times 10^{-4} - 2.1 \times 10^{-8}$	This work
Optical	r'-band	4.83×10^{14}	LCO	58 428	21.38 ± 0.08	46 s	$4.3 \times 10^{-4} - 2.2 \times 10^{-2}$	This work
Optical	i'-band	3.98×10^{14}	LCO	58431–58791	26.6 ± 0.4	∼5d	$4.7 \times 10^{-8} - 2.4 \times 10^{-6}$	This work
Optical	y-band	2.99×10^{14}	LCO	58431–58791	19 ± 3	∼8d	$4.5 \times 10^{-8} - 1.0 \times 10^{-5}$	This work

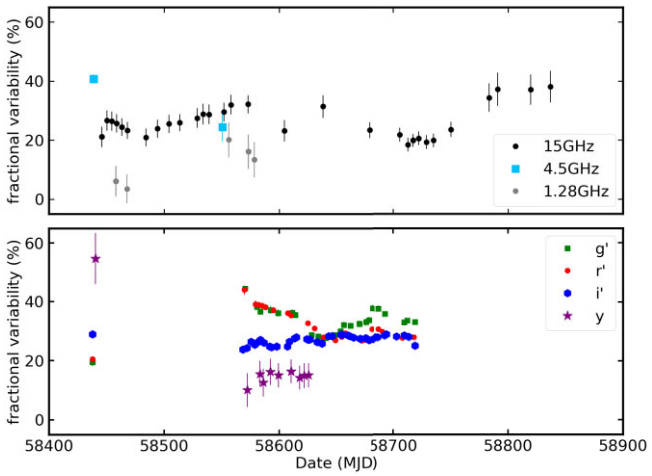

Figure 4. The radio (top panel) and optical (bottom panel) $F_{\rm rms}$ variability as a function of time. We calculate a moving average rms variability with a bin size of 60 d.

(i.e. no contamination from the contaminating star) we measure the average magnitudes of 20.85±0.04, 20.02±0.04, 19.72±0.08, and 19.7±0.3 in the g', r', i', and y bands, respectively.

The middle panel in Fig. 1 shows the long-term radio monitoring from den Eijnden et al. (2020) and Rhodes et al. (2022). Similarly to the optical data, we observe significant variability. We measure rms variability values of 20±4, 46±10, and 33±2 per cent at 1.28, 4.5 and 15.5 GHz, respectively, on week long time-scales. The variability observed at 4.5 GHz appears to be mildly higher; however, we note there are also larger uncertainties; both of these may be the result of a concentrated number of data points at the beginning of the outburst but a low number in total. Like the optical data, we find that the lowest radio frequencies have the smallest $F_{\rm rms}$ values. The levels of variability in the radio band are consistent with that at optical wavelengths, indicating a possible common origin, or related components. After the state transition, denoted by the vertical blue dashed line, we obtain deep radio limits and only a single optical observation was made during the decay into quiescence.

In addition to looking at the outburst-averaged variability properties, we also calculated a 60-d running average of the rms variability for each band. The results are shown in Fig. 4. A 60-d bin size was used such that the only bins with fewer than 3 observations are those that were around periods of Sun-constraint. We found that reducing the bin size to 30 or 45 d amplified potential trends but also increased the uncertainties thus reducing the significance of any variations. Before J1858 was Sun-constrained, we find that the lower frequencies had larger fractional variability values (y and i' bands). After Sun-constraint, this swaps with the highest frequency g' and r'bands demonstrating stronger variability. As the outburst progresses, the variability across all bands becomes very similar at around 30 per cent. The 15 GHz fractional variability smoothly varies between ∼ 20 and ∼ 40 per cent through the outburst, the same range as measured in the g' and r' bands. The 1.3 GHz values systematically sit lower, always below 20 per cent but with much larger uncertainties.

3.2 Spectral energy distributions

For all epochs where observations were made in at least three bands on the same date, we construct optical SEDs, shown in Fig. 5. The optical magnitudes were de-reddened and converted to flux densities. Calculating the contribution of dust along the line of sight is complicated by strong, variable, intrinsic absorption that affects the soft X-rays, with measured neutral hydrogen columns of up to $N_H = (1.4–4.2) \times 10^{23}\,{\rm cm}^{-2}$ (Hare et al. 2020). However, during times when intrinsic absorption was not present, N_H was found to be consistent with the Galactic value (e.g. Hare et al. 2020; Castro Segura et al. 2022; Shahbaz et al. 2023). Using measurements from HI4PI Collaboration (2016), we find that in a 5.5 arcmin region about the source position, the Galactic N_H is $(1.84 \pm 0.03) \times 10^{21}\,{\rm cm}^{-2}$. Absorption coefficients for J1858 were evaluated assuming this value and the Foight et al. (2016) N_H/A_V relation for our Galaxy, resulting in $A_V = 0.64 \pm 0.04$. The optical data were de-reddened using the Cardelli, Clayton & Mathis (1989) extinction law, which adopts extinction values (to be multiplied by A_V) of 1.194, 0.872, 0.666, and 0.438 in the g', r'. i', and y bands, respectively. We note that Castro Segura et al. (2024) derived an extinction of $A_V = 1.00 \pm 0.08$ by fitting the profile of the interstellar absorption feature near 2175 Å in the near-UV spectrum from HST. However, this would translate to (using Foight et al. 2016) a neutral hydrogen column that is significantly higher than the Galactic value. It is possible that dust intrinsic to the system could contribute extra absorption at some orbital phases (see Section 4). For these two reasons, we adopt the Galactic absorption value in the below sections but note any changes that a higher absorption could make to the results. We also note that the much higher, intrinsic, variable neutral hydrogen column of $N_H > 1.4 \times 10^{23}\,cm^{-2}$ does not affect the optical emission. If the dust extinction were to correlate with this intrinsic N_H according to the Foight et al. (2016) law, the resulting in variable absorption would be $\Delta A_V > 48$ which is much higher than the observed amplitude. A similar result was found in the black hole XRB V404 Cyg, which also had strong intrinsic N_H and no corresponding variable A_V seen in optical and UV data (Oates et al. 2019).

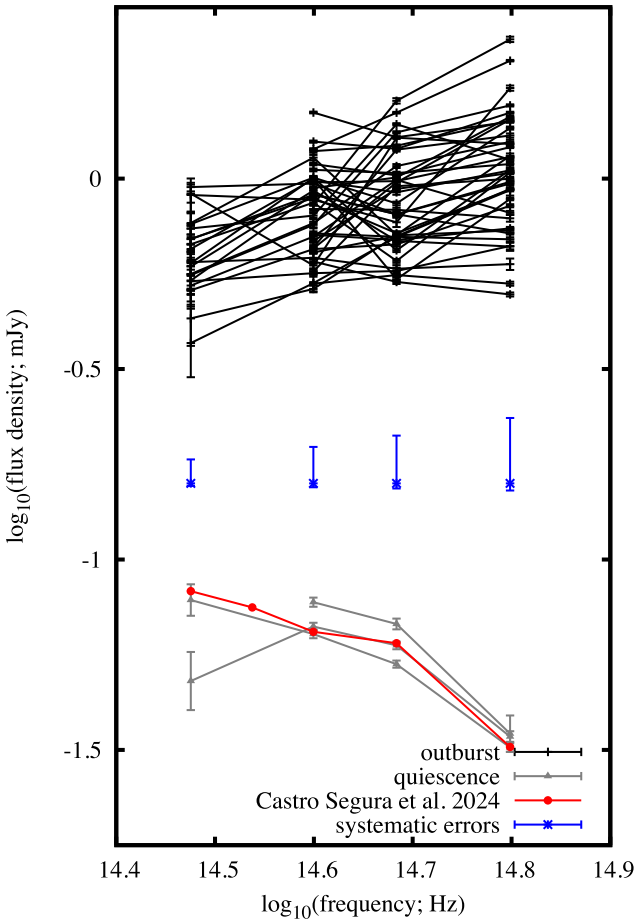

Figure 5. Optical SEDs of J1858 for all epochs where data were collected in at least three bands. The black plus symbols which are the brighter data points, correspond to when the source was in outburst. There are substantial changes in the spectral index during outburst. The fainter grey points (upwards-facing triangles) are from observations taken during quiescence, and we add one SED from the quiescence period before the outburst, taken by Pan-STARRS (Castro Segura et al. 2024). The (blue crosses) systematic errors represent how the SEDs would change with varying extinction. If $A_V = 1.0$ instead of the chosen $A_V = 0.64$ (see Section 3.2) the resulting shift in the data points across the four filters are denoted by the upper blue error bars.

For the data obtained during the outburst, we find that there is a large scatter in the spectral index measurements. Some of the individual SEDs show sharp peaks and troughs within the four bands, which is unphysical and is reflected in the large uncertainties on some of the spectral indices. This is a result of the large amplitude variability demonstrated in Figs 2 and 3 where the source varies on time-scales shorter than the time taken to switch between filters. The continuum emission cannot vary so abruptly within this small wavelength range. Prominent emission and absorption lines could, but they would have to exhibit very high amplitude variability and dominate over the continuum in all bands, which is not expected and such behaviour was not seen in optical spectra (Muñoz-Darias et al. 2020). Combined with the lack of correlation between the magnitudes in different bands, it is not possible to measure long-term changes in the optical spectral index during the outburst. We can, however, estimate an average value for the optical spectral index, which follows $F_\nu \propto \nu^{0.67\pm0.09}$. This is a blue spectrum, which is fairly typical of low-mass X-ray binaries in outburst (e.g. Hynes 2005), despite the

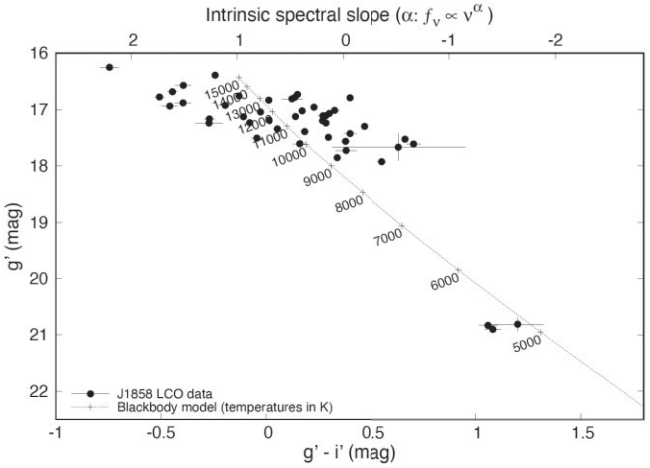

Figure 6. Colour–magnitude diagram of J1858 showing optical brightness g' versus colour g'–i' where the bluer colours that correspond to higher spectral indices are shown to the left, and redder colours are shown to the right, overplotted with a simple model of a single temperature blackbody heating up and cooling denoted by the black dotted line labelled with temperature values.

atypical large amplitude short-term variability. The spectral index values range from $\alpha \sim 1.6$–1.8, which is near the Rayleigh–Jeans limit of a blackbody ($\alpha = 2.0$), to $\alpha \sim -0.6$ to -0.7, which is more consistent with optically thin synchrotron emission. We found that, with some scatter, some of the highest (most positive) spectral index values were when the g'-band flux densities were brightest, and some of the lowest spectral index values were when the g'-band flux densities were faintest as shown in Fig. 6.

We are also able to measure the spectral energy distribution during quiescence. Due to the contamination of the nearby interloper star 2.0 arcsec from J1858, we only include data on dates when solid detections were made (not forced photometry points) and when the seeing was < 1.4 arcsec. This ensured that the MAP photometry was able to exclude the flux from this nearby star from the aperture.

During quiescence, we find that the spectral index is between $\alpha = -1$ and -2, which is consistent with the typical SED of a star or cold, quiescent disc. The SEDs are similar to one derived from Pan-STARRS magnitudes during quiescence before the outburst (Castro Segura et al. 2024), shown by red circles in Fig. 5.

3.3 Colour–magnitude diagram

To analyse the colour evolution of J1858, we constructed a colour–magnitude diagram (CMD) using quasi-simultaneous (observations separated in time by less than 20 min) g' and i'-band LCO data (see Fig. 6). We assume an optical extinction of $A_V = 0.64$ (see Section 3.2) to convert the g'–i' colour into an intrinsic spectral index. We find that when J1858 is fainter in quiescence, it populates the bottom-right corner of the CMD, when the emission could be dominated by the donor star. The source is much brighter and the colour bluer during the outburst, when the emission in LMXBs is expected to be dominated by the accretion disc. We superimpose a blackbody model (Maitra & Bailyn 2008; Russell et al. 2011) depicting the evolution of a single-temperature, constant-area blackbody that has a varying temperature in Fig. 6 (the grey line labelled with temperatures in Kelvin). The normalization of the blackbody model is dependent on the projected surface area of the disc and its luminosity whose parameters are then dependent on

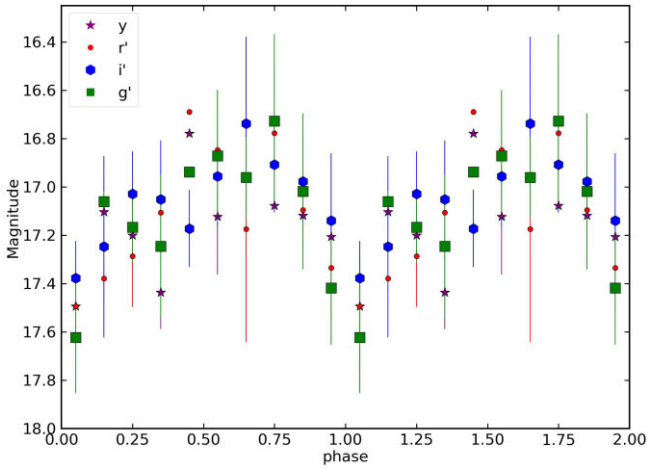

Figure 7. Phase folded light curve for our optical data during the outburst. Each phase bin is 10 per cent of the phase. The uncertainties on each data point reflect the scatter within that phase bin. Points with no error bars only have one observation within that phase bin.

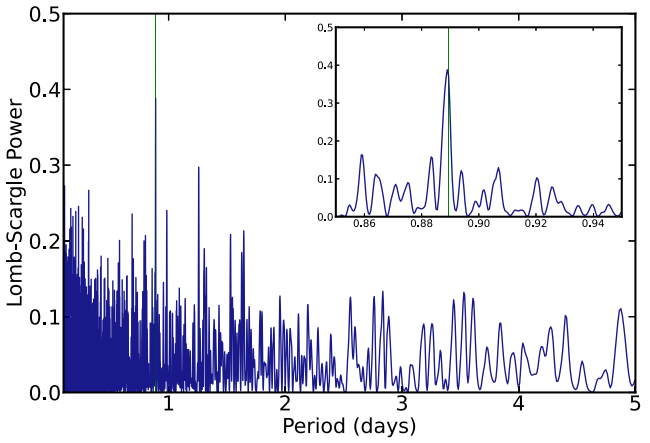

Figure 8. A Lomb–Scargle Periodogram for the optical light-curve data for J1858. Between periods of 0.1 and 5.0 d, we find the strongest peak at 0.889 d with an estimated peak width of 0.001 d (VanderPlas & Ivezić 2015; Vanderplas 2015). This result is consistent with the period derived from eclipse timings in Buisson et al. (2021) denoted with a vertical blue line at 0.88937 d.

several parameters including the accretion disc radius, disc filling factor, distance, and orbital period. The latter two, among others, are well constrained (Buisson et al. 2020a, 2021) whereas others are not and are estimated by marginalizing over when comparing the blackbody model to the data (Zhang et al. 2019; Baglio et al. 2020, 2022; Saikia et al. 2022, 2023b). The temperature corresponding to the optical colours is ∼5000 K during quiescence (which is close to that of the donor star, derived in Castro Segura et al. 2024) and ∼8000–15000 K during outburst, consistent with an ionized disc (hydrogen is completely ionized above 10 000 K; e.g. Lasota 2001) or the dayside of an irradiated companion star (Bassa et al. 2009).

We find that the slope of the model does not approximate the slope in the trend of the data in outburst well. This cannot be due to uncertainty in our optical extinction value (changing $A_V = 0.64$ to $A_V = 1.0$ would make the SEDs slightly bluer but would not be able to account for the shallow slope in the data compared to the model). The shallow slope could imply that a standard thermal (irradiated) disc is not producing all of the optical emission during the outburst, or that the fast variability could be responsible. Since the g' and i' bands are only mildly correlated (Fig. 2), the scatter in the $g' - i'$ colour (∼ 1.5 mag) will be $\sim \sqrt{2}$ times the scatter in each band, spreading the data out more than the blackbody model predicts in the x-axis of Fig. 6. One possible explanation is that an irradiated disc produces the optical emission, but varies on short time-scales due to a highly variable irradiating X-ray flux (as discussed in sections 3.1 and 4 and seen by Shahbaz et al. 2023), leading to scatter in the colour around the mean disc value. This results in the model being a poor approximation of the slope of the trend in the data, although, the model (normalized to the centre of the scattered points) does pass through the quiescent data points which is either a coincidence or lends itself to the possibility of a the disc still contributing in quiescence.

3.4 Periodicity analysis

Given the temporal extent of our monitoring campaign, we folded the optical light curve on the orbital period of the binary: (21.3448±0.0004) h to search for any signs of periodicity (Buisson et al. 2021). We denote phase (ϕ) of 0.0 as the point at superior conjunction of the NS to be consistent with other publications (e.g. Knight et al. 2022, superior conjunction of the NS refers to when the companion star is directly between the observer and the NS). We plot the phase curve for all optical bands (with no correction for extinction) in Fig. 7 and find evidence for phase dependence in all bands. The optical counterpart is brightest between phases of 0.6 and 0.8 and faintest at 0.0 when the NS is being eclipsed. We find that the amplitude modulation is the same (∼0.7 mag) across all bands indicating that a geometry change in the system is causing the phase-dependent changes rather than extinction. This is different from the rms variability measurements, which find that the shortest wavelength bands (g' and r') have the largest rms variability amplitude, which is seen in the large uncertainties on each phase bin.

To ensure that the behaviour we see in Fig. 7 is real, we performed an F-test comparing a flat phase curve and a skewed sinusoid (Israel 2016). We find that the skewed sinusoid model is preferred at a significance level of 99.5 per cent level. We also constructed a Lomb–Scargle Periodogram to search for periodic behaviour in the optical light curve with periods between 0.1 and 5 d (VanderPlas & Ivezić 2015; Vanderplas 2015). The Lomb–Scargle Periodogram is shown in Fig. 8 with a vertical line denoting the orbital period as measured from the eclipses in Buisson et al. (2021). We find a peak at 0.889±0.001 d which is consistent with the measured orbital period of J1858 which is 0.88937±0.00002 d. We note that the orbital period was not given as a prior in the Lomb–Scargle periodogram, which, when combined with the F-test results leads us to conclude that the phase dependence is real.

4 DISCUSSION

Our long-term optical monitoring campaign of J1858 has shown significant variability through the outburst (see Figs 1, 3, and 4). The simplest explanation for the optical behaviour that we observe is that we are randomly sampling the short-time-scale rapid flaring similar to that in Fig. 3 and has been reported elsewhere (Shahbaz et al. 2023; Vincentelli et al. 2023). We compare our long-term data set with the short-term study from Shahbaz et al. (2023) to test this hypothesis. We find that the average magnitude measurements in the g', r', and i' bands are fully consistent; however, comparing the levels of variability between the short (minute) time-scale studies

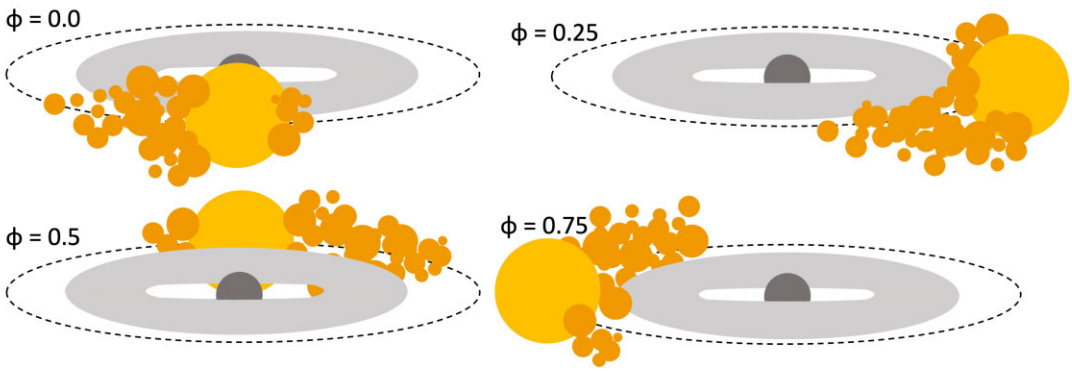

Figure 9. Schematic of how the phase curve (Fig. 7) is produced. At phase 0.7, the projected surface area of the star and ablated material is larger and therefore the reprocessed radiation along the observer's line of sight is larger resulting in a higher flux density. Whereas at phase 0.0, the companion star completely eclipses the NS and so all reprocessed radiation from the star and ablated material travels away from the observer.

from Shahbaz et al. (2023) to our longer (weeks-months) values, we measure slightly lower variability values. In g', r', and i' bands, Shahbaz et al. (2023) measure $F_{\rm rms}$ values of 27, 22, and 23 per cent compared to our 22, 20, and 17 per cent.

Vincentelli et al. (2023) suggest that the variability is a result of changes in mass accretion rate i.e. the system is constantly going through a pattern of ejecting and refilling the inner accretion disc (Belloni et al. 1997). This scenario is expected to result in the repeated ejection of plasmoids each producing radio emission that transitions from optically thick to thin as they expand. High-time-resolution radio observations are needed to resolve individual ejecta that evolve on time-scales of minutes (den Eijnden et al. 2020; Rhodes et al. 2022; Vincentelli et al. 2023). In Rhodes et al. (2022) and Vincentelli et al. (2023), high-time-resolution radio observations showed a highly variable radio source that transitioned from optically thick to thin over time-scales of minutes as would be expected for repeated rapid ejections. Observations that lasted longer than 15 min were averaging over multiple evolving plasmoids producing a flat/optically thick variable radio source, as is shown in the lower panel of Fig. 1. Therefore, although we cannot directly correlate the behaviour between optical and radio bands, we can connect the variability observed at optical wavelengths due to a varying accretion rate to that at radio frequencies due to changing jet power that continues throughout the outburst.

The above statements assume that the jet dominates emission only at radio frequencies; however, depending on the relative strength of different ejecta, the contribution at higher frequencies may begin to dominate over the emission from the disc or irradiated stellar companion. The optical spectral index, if jet/ejecta dominated, would follow $F_\nu \propto \nu^{<0}$. We measure negative spectral indices in eight observations during the outburst. The flux densities of the optical emission are high enough ($\sim$1 mJy) that it would be possible that the optical and radio emission (100s μJy with an optically thick spectral index) could originate from the same process i.e. synchrotron emission from the jet. Therefore, we find it likely that there is also a jet contribution to the optical variability.

One of the most interesting discoveries from this observing campaign is the apparent phase dependence in the optical light-curve data (Fig. 7). A possible interpretation of the phase-dependent behaviour is a superhump, which is thought to occur due to precession in the disc (Whitehurst & King 1991). The period of the superhump is expected to be close to or a few per cent different to the orbital period and so could be visible in the orbital phase curve. We rule out the possibility of a superhump based on the maximum difference between the brightest and faintest points in the phase curves shown in Fig. 7 being about 0.7 mag. This is larger than the largest modulation amplitude (0.5 mag) found to date caused by a superhump which was found in MAXI J1820−070, a BH LMXB (Thomas et al. 2022). Furthermore, the period of a superhump is expected to evolve as the outburst progresses which we find no evidence of in J1858, thus making a superhump even less likely as the origin of the phase variability.

Instead, we interpret the orbital modulation as a result of irradiation within the system. From Buisson et al. (2021) and Knight et al. (2022), we know that the system has a high inclination (i.e. is almost edge-on) and given the results from Vincentelli et al. (2023) and Knight et al. (2023), where strong irradiation is inferred, one would expect the optical phase curve to be sinusoidal. However, the observed phase curve deviates from a sinusoid with the peak occurring at $\phi \approx 0.7$ rather than 0.5 and the minimum occurring at $\phi \approx 0.0$. We interpret the asymmetry as the result of additional material gravitationally bound to the system. The material is thought to be removed from the stellar companion as a result of high energy radiation from the inner accretion flow irradiating the companion. Extended material has been invoked in radio and X-ray observations from spider pulsars and other X-ray binaries, respectively (Fruchter, Stinebring & Taylor 1988; Knight et al. 2023).

To determine how the ablated material is changing the phase curve, we compare the amplitude of the modulation in Fig. 7 across all four wavebands. We find no colour dependence in the phase curve shape: the difference between the peak and trough across all bands is about 0.7 magnitudes. If the shape was due to dust absorption of light by ablated material, we would expect the amplitude of the phase curve to be 2.7 times greater at g' than y band. No such dependence is observed. A flat frequency dependence could be a result of complete obscuration; however the magnitude decrease around phase 0.0 is not sufficient for complete obscuration.

Instead, we hypothesize that the peak in the phase curve is caused by increased projected surface area for reprocessing of the X-ray emission from the inner accretion disc into our line of sight. A schematic of this scenario is shown in Fig. 9. At $\phi = 0.0$, the NS is being eclipsed by the companion star, the disc is not completely obscured by the companion/ablated material which is why the flux level at phase 0.0 does not drop as low as in quiescence. Because the compassion star is between us and the neutron star, we do not observe any reprocessed emission. Between phase 0.0 to $\sim$0.6, the sky-projected area available for reprocessing hard X-ray emission into our line of sight slowly increases to a maximum around 0.7

where the ablated material nor the star is blocked by the disc. The system appears brightest when the surface area is largest and so there is more X-ray radiation being reprocessed into our line of sight (see $\phi = 0.75$ in Fig. 9). Between phases 0.7 and 1.0, we observe less reprocessed material because the apparent size of the star and ablated material is smaller as the material sits behind the star according to our viewing angle and so the system appears fainter.

Phase folding of X-ray binary optical light curves is usually performed when the source is in quiescence in order to study the ellipsoidal modulation of the companion (Avni & Bahcall 1975). The behaviour we observed cannot be explained by ellipsoidal modulation. Instead, the behaviour we observe here is very similar to that observed in transitional millisecond pulsars (e.g. Stringer et al. 2021; de Martino et al. 2024). The phase dependence is often concluded to be due to irradiation of the companion with no need for ablation to explain the data. Evidence for ablation in neutron star systems was first found in eclipsing millisecond pulsars called spider pulsars, where there is an increased density of material around the ingress and egress of the pulsar eclipse (Fruchter et al. 1988; Polzin et al. 2019), and more recently in neutron star X-ray binaries (Knight et al. 2023). In the case of spider pulsars, the mass-loss rates inferred from the ablation will only just, or is insufficient, to fully evaporate the stellar companion within a Hubble time, which creates problems if spider pulsars are the progenitors of isolated millisecond pulsars (Ginzburg & Quataert 2020; Polzin et al. 2020). Our observations, which we interpret as ablated material extended around the binary orbit throughout the outburst, provide a possible path to increase the total time over which evaporation of the companion can occur and therefore make isolated millisecond pulsars easier to produce.

5 SUMMARY AND CONCLUSIONS

In this paper, we have presented a long-term optical monitoring campaign for the NS LMXB *Swift* J1858.6–0814 both in outburst and after in quiescence. Our observations show significant frequency-dependent variability throughout the outburst. We compare variability observed in the weekly optical and radio observations (the latter from den Eijnden et al. 2020; Rhodes et al. 2022) and find that the variability amplitude is similar indicating that the cause of the variability is likely to be a common process in the two bands: a result of changes in mass accretion rate. We have also shown that there are processes ongoing within the J1858 system that affect the optical emission on other time-scales: the jet flares that last less than 15 min (Rhodes et al. 2022; Vincentelli et al. 2023) and phase-dependent behaviour on time-scales of hours and so the lack of a good fit for a single black body emitting region as shown in Fig. 6 is expected.

By folding the optical data about the orbital period, we find significant orbital modulation that disappears in quiescence. Such behaviour is reminiscent of spider pulsars, where the pulsar wind ablates material from the surface of the stellar companion and reduces its mass. However, unlike in spider pulsars, our observations find evidence for ablation while the NS system is actively accreting as an LMXB, thus providing a longer timescale over which a stellar companion could be destroyed and leave behind an isolated MSP.

ACKNOWLEDGEMENTS

We thank the anonymous referee for their help in improving the manuscript. We thank Dan Bramich for his contributions to the development of the XB-NEWS pipeline, and for insightful discussions. AHK acknowledges support from the Science and Technology Facilities Council (STFC) as part of the consolidated grant award ST/X001075/1. JvdE acknowledges a Warwick Astrophysics prize post-doctoral fellowship made possible thanks to a generous philanthropic donation. This work uses data from the Faulkes Telescope Project, which is an education partner of Las Cumbres Observatory (LCO). The Faulkes Telescopes are maintained and operated by LCO. This material is based upon work supported by Tamkeen under the NYU Abu Dhabi Research Institute grant CASS. MCB acknowledges support from the INAF-Astrofit fellowship.

DATA AVAILABILITY

The optical data from Faulkes/LCO underlying this article will be shared on reasonable request to the corresponding author.

REFERENCES

Alpar M. A., Cheng A. F., Ruderman M. A., Shaham J., 1982, Nature, 300, 728
Archibald A. M. et al., 2009, Science, 324, 1411
Avni Y., Bahcall J. N., 1975, ApJ, 197, 675
Baglio M. C., D'Avanzo P., Muñoz-Darias T., Breton R. P., Campana S., 2013, A&A, 559, A42
Baglio M. C. et al., 2017, A&A, 600, A109
Baglio M. C., Russell D. M., Pirbhoy S., Bahramian A., Heinke C. O., Roche P., Lewis F., 2018, Astron. Telegram, 12180, 1
Baglio M. C. et al., 2020, ApJ, 905, 87
Baglio M. C. et al., 2022, ApJ, 930, 20
Bagnoli T., in't Zand J. J. M., D'Angelo C. R., Galloway D. K., 2015, MNRAS, 449, 268
Bahramian A., Degenaar N., 2023, in, Bambi C., Santangelo A., Handbook of X-ray and Gamma-ray Astrophysics. Edited by Cosimo Bambi and Andrea Santangelo. Springer, Singapore, p. 120
Bassa C. G., Jonker P. G., Steeghs D., Torres M. A. P., 2009, MNRAS, 399, 2055
Belloni T., Méndez M., King A. R., van der Klis M., van Paradijs J., 1997, ApJ, 479, L145
Bramich D. M., Freudling W., 2012, MNRAS, 424, 1584
Bright J., Fender R., Motta S., Rhodes L., Titterington D., Perrott Y., 2018, Astron. Telegram, 12184, 1
Brown T. M. et al., 2013, PASP, 125, 1031
Buisson D. J. K. et al., 2020a, MNRAS, 499, 793
Buisson D. J. K., Altamirano D., Remillard R., Arzoumanian Z., Gendreau K., Gandhi P., Vincentelli F., 2020b, Astron. Telegram, 13536, 1
Buisson D. J. K. et al., 2021, MNRAS, 503, 5600
Cantrell A. G. et al., 2010, ApJ, 710, 1127
Cardelli J. A., Clayton G. C., Mathis J. S., 1989, ApJ, 345, 245
Carotenuto F. et al., 2021, MNRAS, 504, 444
Casella P. et al., 2010, MNRAS, 404, L21
Castro Segura N. et al., 2022, Nature, 603, 52
Castro Segura N. et al., 2024, MNRAS, 527, 2508
Corbel S., Fender R. P., 2002, ApJ, 573, L35
de Martino D. et al., 2024, A&A, 691, A36
Fender R. P., 2001, MNRAS, 322, 31
Fender R. P., Belloni T. M., Gallo E., 2004, MNRAS, 355, 1105
Foight D. R., Güver T., Özel F., Slane P. O., 2016, ApJ, 826, 66
Fruchter A. S., Stinebring D. R., Taylor J. H., 1988, Nature, 333, 237
Gandhi P. et al., 2017, Nat. Astron., 1, 859
Ginzburg S., Quataert E., 2020, MNRAS, 495, 3656
Goodwin A. J. et al., 2020a, MNRAS, 498, 3429
Goodwin A. J. et al., 2020b, MNRAS, 498, 3429
Greene J., Bailyn C. D., Orosz J. A., 2001, ApJ, 554, 1290
Greenhill J. G., Giles A. B., Coutures C., 2006, MNRAS, 370, 1303
Gusinskaia N. V. et al., 2017, MNRAS, 470, 1871
HI4PI Collaboration, 2016, A&A, 594, A116
Hare J. et al., 2020, ApJ, 890, 57
Hynes R. I., 2005, ApJ, 623, 1026

Ingram A. R., Motta S. E., 2019, New Astron. Rev., 85, 101524
Israel R., 2016, Personal communication
Kennea J. A., Krimm H. A., 2018, Astron. Telegram, 12160, 1
Knight A. H., Ingram A., Middleton M., 2022, MNRAS, 514, 1908
Knight A. H., Ingram A., van den Eijnden J., Buisson D. J. K., Rhodes L., Middleton M., 2023, MNRAS, 520, 3416
Krimm H. A. et al., 2018, Astron. Telegram, 12151, 1
Lasota J.-P., 2001, New Astron. Rev., 45, 449
Lewis F., 2018, in Fitzgerald M., James C. R., Buxner S., White S., eds, Robotic Telescope, Student Research and Education Proceedings, Vol. 1. San Diego, California, USA, p. 237
Lewis F., Russell D. M., Fender R. P., Roche P., Clark J. S., 2008, preprint (arXiv:0811.2336)
Maitra D., Bailyn C. D., 2008, ApJ, 688, 537
Malzac J. et al., 2018, MNRAS, 480, 2054
Migliari S., Fender R. P., Rupen M., Wachter S., Jonker P. G., Homan J., van der Klis M., 2004, MNRAS, 351, 186
Muñoz-Darias T. et al., 2013, MNRAS, 432, 1133
Muñoz-Darias T. et al., 2020, ApJ, 893, L19
Oates S. R. et al., 2019, MNRAS, 488, 4843
Paice J. A., Gandhi P., Dhillon V. S., Marsh T. R., Green M., Breedt E., 2018, Astron. Telegram, 12197, 1
Papitto A. et al., 2013, Nature, 501, 517
Parikh A. S., Wijnands R., Altamirano D., 2020, Astron. Telegram, 13725, 1
Plotkin R. M. et al., 2016, MNRAS, 456, 2707
Polzin E. J., Breton R. P., Stappers B. W., Bhattacharyya B., Janssen G. H., Osłowski S., Roberts M. S. E., Sobey C., 2019, MNRAS, 490, 889
Polzin E. J., Breton R. P., Bhattacharyya B., Scholte D., Sobey C., Stappers B. W., 2020, MNRAS, 494, 2948
Rahoui F. et al., 2012, MNRAS, 422, 2202
Rajwade K., Kennedy M., Breton R., Stappers B., Sanpa-arsa S., Irawati P., Dhillon V., Marsh T., 2018, Astron. Telegram, 12186, 1
Rhodes L., Fender R. P., Motta S., van den Eijnden J., Williams D. R. A., Bright J., Sivakoff G. R., 2022, MNRAS, 513, 2708
Roberts M. S. E., 2012, Proc. IAU Symp. Vol. 8, Surrounded by Spiders! New Black Widows and Redbacks in the Galactic Field, Kluwer, Dordrecht, p. 127
Russell D. M., Fender R. P., Jonker P. G., 2007, MNRAS, 379, 1108
Russell D. M., Casella P., Fender R., Soleri P., Pretorius M. L., Lewis F., van der Klis M., 2011, preprint (arXiv:1104.0837)
Russell D. M., Qasim A. A., Bernardini F., Plotkin R. M., Lewis F., Koljonen K. I. I., Yang Y.-J., 2018, ApJ, 852, 90
Russell D. M. et al., 2019, Astron. Nachr., 340, 278
Saikia P., Russell D. M., Baglio M. C., Bramich D. M., Lewis F., 2020, Astron. Telegram, 13719, 1
Saikia P. et al., 2022, ApJ, 932, 38
Saikia P., Russell D. M., Pirbhoy S. F., Baglio M. C., Bramich D. M., Alabarta K., Lewis F., Charles P., 2023a, MNRAS, 524, 4543
Saikia P., Russell D. M., Pirbhoy S. F., Baglio M. C., Bramich D. M., Alabarta K., Lewis F., Charles P., 2023b, ApJ, 949, 104
Shahbaz T. et al., 2023, MNRAS, 520, 542
Stappers B. W., Bailes M., Lyne A. G., Camilo F., Manchester R. N., Sandhu J. S., Toscano M., Bell J. F., 2001, MNRAS, 321, 576
Stringer J. G. et al., 2021, MNRAS, 507, 2174
Tetarenko A. J., Casella P., Miller-Jones J. C. A., Sivakoff G. R., Tetarenko B. E., Maccarone T. J., Gandhi P., Eikenberry S., 2019, MNRAS, 484, 2987
Thomas J. K. et al., 2022, MNRAS, 513, L35
Tonry J. L. et al., 2018, ApJ, 867, 105
VanderPlas J. T., Ivezić Ž., 2015, ApJ, 812, 18
Vanderplas J., 2015, gatspy: General Tools for Astronomical Time Series in Python, https://doi.org/10.5281/zenodo.14833
Vasilopoulos G., Bailyn C., Milburn J., 2018, Astron. Telegram, 12164, 1
Vaughan S., Edelson R., Warwick R. S., Uttley P., 2003, MNRAS, 345, 1271
Veledina A., Poutanen J., Vurm I., 2011, ApJ, 737, L17
van den Eijnden J. et al., 2020, MNRAS, 496, 4127
Vincentelli F. M. et al., 2023, Nature, 615, 45
Whitehurst R., King A., 1991, MNRAS, 249, 25
Wijnands R., van der Klis M., 1998, Nature, 394, 344
Zhang G. B. et al., 2019, ApJ, 876, 5
Zurita C., Casares J., Shahbaz T., 2003, ApJ, 582, 369

This paper has been typeset from a TEX/LATEX file prepared by the author.